VICTORIA UNIVERSITY
MELBOURNE AUSTRALIA

Impacts of future urban expansion on urban heat island effects during heatwave events in the city of Melbourne in southeast Australia

This is the Published version of the following publication

RESEARCH ARTICLE

Impacts of future urban expansion on urban heat island effects during heatwave events in the city of Melbourne in southeast Australia

Hosen M. Imran[1,2,3] | Jatin Kala[4] | Anne W. M. Ng[1,3] | Shobha Muthukumaran[1,3]

[1]College of Engineering and Science, Victoria University, Melbourne, Victoria, Australia

[2]Institute of Water and Environment, Dhaka University of Engineering & Technology, Gazipur, Bangladesh

[3]Institute for Sustainable Industries & Livable Cities, Victoria University, Melbourne, Victoria, Australia

[4]Environmental and Conservation Sciences, Murdoch University, Perth, Western Australia, Australia

Correspondence
Hosen M. Imran, College of Engineering and Science, Victoria University, PO Box 14428, Melbourne, Victoria, Australia.
Email: ihosen83@gmail.com

Abstract

The city of Melbourne in southeast Australia is planning to expand urban areas substantially by the year 2050 and this expansion has the potential to alter the Urban Heat Island (UHI), that is, higher temperatures in urban areas as compared to surrounding rural areas. Moreover, Melbourne has been experiencing more frequent heatwaves for last two decades, and the intensity and duration of heatwaves is expected to increase in the future, which could exacerbate the UHI. This study evaluates the potential impacts of future urban expansion on the urban meteorology in Melbourne city during four of the most severe heatwave events during the period 2000–2009. Urban expansion is implemented as high-density urban with a high urban fraction of 0.9 to investigate the maximum possible impact. Simulations are carried out using the Weather Research and Forecasting model coupled with the Single-Layer Urban Canopy Model with current land-use and future urban expansion scenarios. Urban expansion increases the near-surface (2-m) UHI (UHI_2) by 0.75 to 2.80 °C and the skin-surface UHI (UHI_{sk}) by 1.9 to 5.4 °C over the expanded urban areas during the night, with no changes in existing urban areas. No substantial changes in UHI_2 and UHI_{sk} occur during the day over both existing and expanded urban areas. This is largely driven by changes in the storage heat flux, with an increase in storage heat at night and a decrease during the day; that is, excess storage heat accumulated during the day is released at night, which causes a slower decrease of near-surface temperature and increase in the UHI. Urban expansion did not affect human thermal comfort (HTC) in existing urban areas and there were no marked differences in HTC between existing and expanded urban areas.

KEYWORDS
coupled WRF–SLUCM model, human thermal comfort, urban expansion, urban heat island

1 | INTRODUCTION

Changes in land cover due to increased urbanization can affect the urban environment and climate substantially (Seto and Shepherd, 2009). One well-documented effect of urbanization is the Urban Heat Island (UHI); that is, higher temperatures in urban areas compared with surrounding rural areas, particularly during the night (Arnfield, 2003). Urban expansion has the potential to enhance UHI effects further (for example, Pauleit *et al.*, 2005; Argüeso *et al.*, 2014; Yang *et al.*, 2016; Morris *et al.*, 2011; Liu *et al.*, 2018) and hence understanding the impacts of future urban expansion on the UHI is very important. A number of features, such as building fabric, building form, thermal properties of construction materials, synoptic condition and wind flow, and anthropogenic heat, combine to generate the UHI in urban areas (Oke *et al.*, 1991; Harman and Belcher, 2006). The UHI is driven by the higher thermal heat capacity and heat storage of urban infrastructure and reduced evapotranspiration due to the loss of vegetation and increase in impermeable surfaces. The UHI results in higher air temperatures at screen level in urban areas that can contribute to heat-related illnesses including heart disease, which can lead to mortality, particularly during summer, and these effects can be exacerbated during heatwaves in Australia (Department of Infrastructure and Regional Development, 2013). For example, the deaths of a total of 4,555 people were attributed to extreme heat over the period 1900–2011 in Australia, which is 55.2% of the total natural hazard deaths (Coates *et al.*, 2014). In addition, higher temperatures in urban areas also affect urban ecosystems, as well as human thermal comfort, and increase the rate of energy consumption (Block *et al.*, 2012).

Melbourne is the fastest growing city in Australia and, according to Plan Melbourne 2050, the urban area is expected to expand into the surrounding suburban regions (more details about plan Melbourne is available at http://www.planmelbourne.vic.gov.au/the-plan). The urbanization rate in Melbourne metropolitan areas is increasing rapidly, with the projected population of Melbourne expected to increase from 3.5 million to reach 8 million by 2056 (Australian Bureau of Statistics, 2008). Moreover, studies predict more frequent and longer lasting heatwaves over eastern Australia (Perkins-Kirkpatrick *et al.*, 2016), and UHI effects are likely to be most pronounced during such events (Liu *et al.*, 2018). The rapid expansion of urban areas is continuing within the metropolitan area, which will play an important role in the development of this city in future.

Coutts *et al.* (2008) investigated the impacts of long-term urban planning strategies according to Plan Melbourne 2030 on the local climate and above-canopy UHI during the Austral summer for the month of January in 2004 (current urban scenario) and 2030 (future urban scenario) in the city of Melbourne by using The Air Pollution Model (TAPM: Hurley, 2000). They showed that urban expansion according to plan Melbourne 2030 would likely lead to a more intense UHI during the night, with effects during the day being less significant. An earlier study by Coutts *et al.* (2007) examined the impacts of urban density on the surface energy balance for the city of Melbourne and showed that increasing urban fractions led to higher nocturnal temperatures. A number of studies have used climate models for urbanization-related climate studies at different spatial scales (global, regional: Wang *et al.*, 2012; Zhao *et al.*, 2013; Liao *et al.*, 2014; Wang *et al.*, 2015), and these studies also report higher near-surface air temperature due to increased urbanization. However, the impacts of urban expansion during heatwave events are largely unknown.

The impacts of urbanization on the UHI can be investigated from meteorological observations as well as remote sensing data. However, a number of atmospheric models now include explicit urban canopy schemes that incorporate complex urban parametrizations and this can be a useful tool in sustainable urban planning. Hence, numerical weather and climate models are increasingly used to assess the impacts of urbanization (both current and future) on weather and climate at global and regional scales (for example, Chen *et al.*, 2014). A commonly used numerical modeling tool is Weather Research and Forecasting (WRF: Skamarock *et al.*, 2005), coupled to the Single-Layer Urban Canopy Model (SLUCM: Kusaka *et al.*, 2001), which has been used to investigate the response of urban meteorology to land-use changes, including urbanization, in major metropolitan cities such as Guangzhou, China (Meng *et al.*, 2011), New York USA (Holt and Pullen, 2007), and Sydney in eastern Australia (Argüeso *et al.*, 2014).

Careful urban planning can be a useful mitigation strategy in reducing the adverse impacts of urbanization and improving urban climate and human health (Stone *et al.*, 2010). According to Adachi *et al.* (2014), a compacted city has a higher potential to increase the mean UHI effects compared with a sparse city. Changes in urban structures vary between different cities and the mitigation of heat-related risks varies according to different urban structures (Oke, 1981; Frolking *et al.*, 2013). Therefore, the impacts of future urbanization on the city and neighborhood scales need to be included in urban design and development plans. The aim of this study is to investigate the impacts of increased urbanization according to plan Melbourne 2050 on the urban meteorology during heatwave events. The study focuses on the physical mechanisms, which play key roles in affecting key atmospheric variables as a result of urban expansion. Although this study is limited to one particular city, the overall principles will be relevant elsewhere for other cities that experience a similar climate.
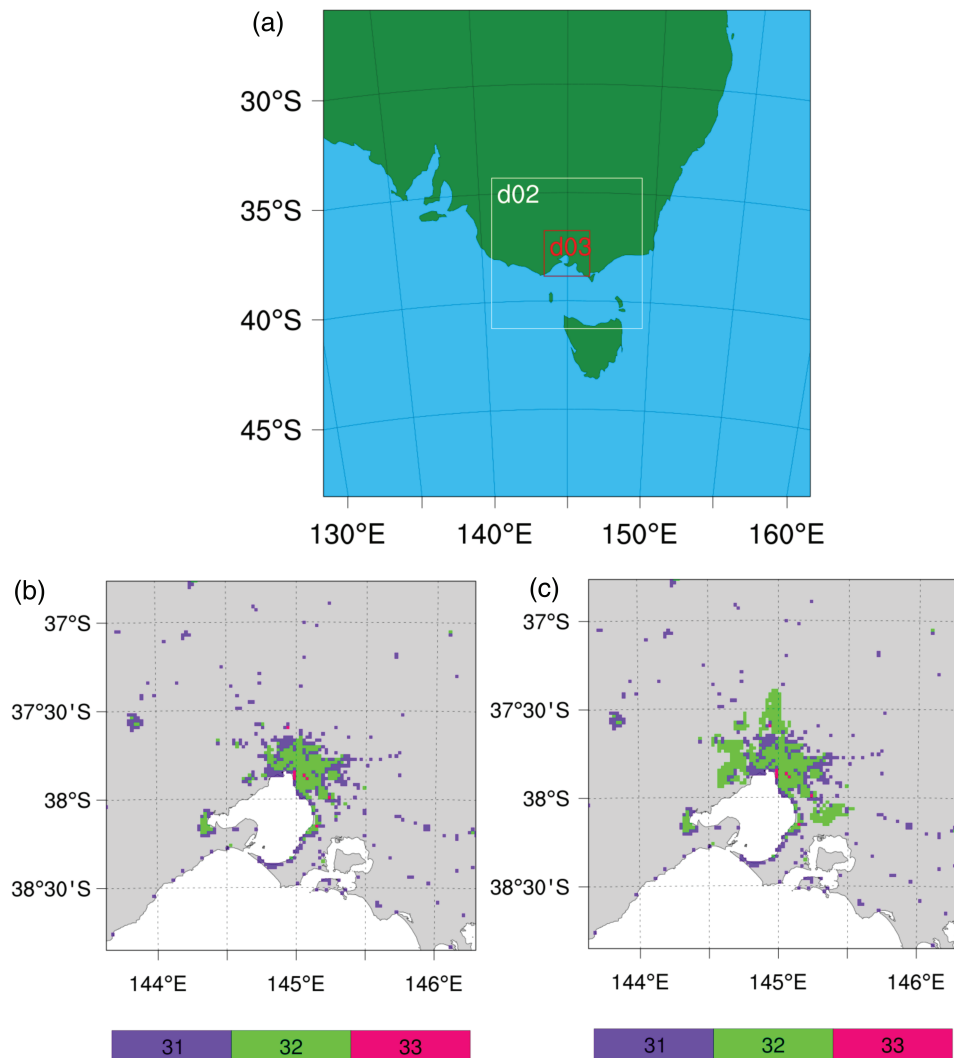
2 | METHODOLOGY

2.1 | Urban planning strategy/projections of Plan Melbourne 2050

The Victorian Government has introduced an urban planning strategy titled "Plan Melbourne 2050" to accommodate the increasing population. The Plan Melbourne 2050 urban expansion data can be obtained from the Environment, Land, Water and Planning Department of the Victoria State Government (http://www.planmelbourne.vic.gov.au/maps). This plan describes the future shape of the city of Melbourne over the next 33 years, with the new wave of urban growth expected to spread to the outer suburban area, especially in the west, north, and southeast of the city (Figure 1c).

The anticipated urban development could affect Melbourne's built and natural environment and could potentially increase UHI effects if urban development is not planned in a careful manner. The city of Melbourne has already faced several extreme heatwave events, during which maximum temperatures reached 45.1 and 43.9 °C during 2009 and 2014, respectively. During summer, prevailing anticyclonic conditions can lead to heatwaves, which bring dry and warm air over the city, exacerbating urban temperatures (Nicholls and Larsen, 2011; Nairn and Fawcett, 2011). Summer heatwaves can lead to temperatures in excess of 35 °C, while the mean UHI intensity is estimated at 3.56 °C in the early morning (6 a.m. local time) during these heatwave events in Melbourne (Morris and Simmonds, 2000). However, the UHI intensity can be much higher than the mean UHI under optimal conditions, such as clear skies and low winds. A maximum UHI of 7.1 °C has been observed in the central business district of Melbourne at 9 p.m. (local time) from an automobile transect carried out in 1992 (Torok et al., 2001).

FIGURE 1 (a) Model nested domain configuration (the boundary represents the outer domain with a resolution of 18 km, and d02 and d03 denote the boundaries of the two inner nested domains, with resolutions of 6 and 2 km respectively), (b) current distribution of urban land use, (c) high-density urban expansion according to Plan Melbourne 2050. The numbers 31, 32, and 33 represent the low-density urban, high-density urban, and commercial/industrial areas, respectively

2.2 | Case studies

The study investigates the impacts of urban expansion during severe heatwave events, as heat stress is more likely during such events. Following Imran *et al.* (2018b), who evaluated the WRF model coupled to the SLUCM in simulating heatwave events over southeast Australia, this study focuses on four heatwave events, which were the most severe over the city of Melbourne during the period 2000–2009. These events occurred in 2000 (2–4 February), 2006 (20–22 January), 2007 (16–18 February) and 2009 (28–30 January). Event 4 was the most severe among these four heatwave events. It led to the Black Saturday bushfires (one of the largest bushfire events in Australia's history, which led to a large number of fatalities) in early February 2009 (Engel *et al.*, 2013).

2.3 | WRF model setup and experiments

This WRF model is commonly used for urban meteorology studies (for example, Argüeso *et al.*, 2014; Chen *et al.*, 2014; Sharma *et al.*, 2016; Morris *et al.*, 2011) and the version used in this study is WRFv3.8.1. The model was used to simulate the four heatwave events with present urban land use (control simulations) and experiments were carried out using the 2050 urban land-use scenarios over the city of Melbourne in southeast Australia. The initial and boundary conditions were obtained from six-hourly ERA-Interim reanalysis data (Dee *et al.*, 2011). Three two-way nested domains with horizontal grid resolutions of 18, 6, and 2 km were used (Figure 1a). The innermost domain (D03) mainly covers the city of Melbourne and surrounding rural areas. A total of 38 vertical levels were used, closely spaced in the boundary layer and further apart in the upper atmosphere. Following Imran *et al.* (2018a), the first 24 hr of the simulation period is considered as spin-up time and the remaining 72 hr of simulations are used for analyses.

The choice of physics parametrizations was based on Imran *et al.* (2018b), who conducted an extensive sensitivity analysis of WRF to different physics options in simulating the same four heatwave events over the city of Melbourne. Imran *et al.* (2018b) evaluated a number of physics options by comparing WRF simulations against station, gridded, and atmospheric sounding observations. In addition, they carried out an analysis of the physical processes and dynamics associated with the four heatwave events and showed that the WRF model is able to simulate various climate variables (for example, temperature, relative humidity, wind speed) and UHI over the city of Melbourne. This choice of physical parametrizations includes the Thompson microphysics scheme (Thompson *et al.*, 2008), the rapid radiative transfer model for general circulation models shortwave and longwave radiation schemes (Iacono *et al.*, 2008), the Mellor-Yamada-Janjić planetary boundary layer (PBL) scheme (Janjic, 1994), the Monin–Obukhov surface layer

scheme, the Noah land-surface model (Chen and Dudhia, 2001), and the Grell-3D cumulus scheme (Grell and Dévényi, 2002). No cumulus scheme was used for the innermost domain, because a resolution of 2 km is sufficient to resolve convection. We do not carry out model evaluation in this article, as extensive evaluation is documented in Imran *et al.* (2018b) for the same four heatwave events, as well as in Imran *et al.* (2018a), who conducted further comparisons of WRF-SLUCM winds and temperature against station observations for the most severe event out of the four case studies.

The SLUCM was used to parametrize the physical urban processes, which represent energy and momentum exchange between urban surfaces (for example, roofs, walls, and roads) and the atmosphere (Kusaka *et al.*, 2001). The default representation of urban land use in WRF was replaced by the Jackson *et al.* (2010) urban dataset for representing the current spatial distribution of low-density, high-density, and commercial/industrial areas in the city of Melbourne. The Jackson *et al.* (2010) data is a global dataset of four urban categories (low-density urban, medium-density urban, high-density urban, and tall building areas) and also includes properties of urban extent, urban morphology, and thermal and radiative properties of building materials. It is specifically designed for use in urban meteorology and climatological studies. The four urban categories from the Jackson *et al.* (2010) urban land-use data were converted into the three categories (low-density, high-density, and commercial/industrial) based on the 24 United States Geological Survey (USGS) land use categories, as used by the SLUCM in the WRF model. We note that other land-use databases can be used in WRF, for example, MODIS. Our choice of the USGS database is based on our previous studies (Imran *et al.*, 2018a, 2018b), which showed that WRF was able to simulate the heatwave events adequately when compared with meteorological stations in the urban area. The low- and medium-density urban categories of the Jackson *et al.* (2010) land-use dataset were classified as low- and high-density urban areas, respectively, while the high-density urban areas and tall buildings were classified as commercial/industrial areas, as illustrated in Figure 1b. These reclassifications allow for a realistic representation of urban land-use categories for this city. Only urban grid cells were modified and the remaining grid cells were kept the same as the default WRF land-use data. Figure 1b shows the current distribution of urban land use and Figure 1c shows the future urban expansion scenario based on Plan Melbourne 2050. Following the previous study by Argueso *et al.* (2014), who investigated the impacts of future urban expansion in the city of Sydney in eastern Australia using WRF-SLUCM, all future urban expansion (Figure 1c) was classified as high-density urban. A similar approach has been used to investigate the impacts of future climate change and urban expansion for US cities using the coupled WRF-SLUCM model (Krayenhoff *et al.*, 2018).

TABLE 1 Urban properties for low-density, high-density, and commercial/industrial areas used by the SLUCM in WRF

Properties/parameters	Low-density urban	High-density urban	Commercial/industrial
Built/impervious fraction	0.70 (default 0.50)	0.90	0.95
Roof width (Rf)	8.3 m	9.4 m	10 m
Road width (Rd)	8.3 m	9.4 m	10 m
Roof fraction in built/impervious part [Rf/(Rf + Rd)]	50%	50%	50%
Roof fraction in whole urban grid	25%	45%	47.5%
Building height	5 m	7.5 m	10 m

The urban morphological properties for all simulations use the default setup in the WRF model, except the urban fraction for low-density urban areas (Table 1), which was increased from 0.5 to 0.7. Default urban fractions are included in the SLUCM for three urban categories, which may not necessarily be representative for a specific city. Using urban fractions of 0.50 and 0.70 showed that the results were more realistic when using an urban fraction of 0.7 for low-density urban areas, and this is consistent with a study focusing on the UHI in Melbourne by Coutts *et al.* (2007), who derived urban fractions using the Geographic Information System and aerial photography. Following Coutts *et al.* (2007), other studies have also used same urban fraction 0.70 for low-density urban areas in evaluating UHI effects in the city of Melbourne (Jacobs *et al.*, 2017; Jacobs *et al.*, 2018; Imran *et al.*, 2018a). The use of a higher urban fraction compared with default values is also consistent with other studies that have used WRF-SLUCM in UHI studies for cities in China (Chen and Frauenfeld, 2016) and the city of Sydney in southeast Australia (Argueso *et al.*, 2014).

2.4 | Numerical experiments

The impacts of urban expansion are explored by incorporating high-density urban expansion over the rural areas based on the proposed urban expansion strategy of Plan Melbourne 2050. A total of eight numerical simulations were conducted: four control experiments with current urban land use (Figure 1b), and four experiments with high-density urban expansion according to plan Melbourne 2050 (Figure 1c). All simulations used the same initial and boundary conditions from the ERA-Interim reanalysis.

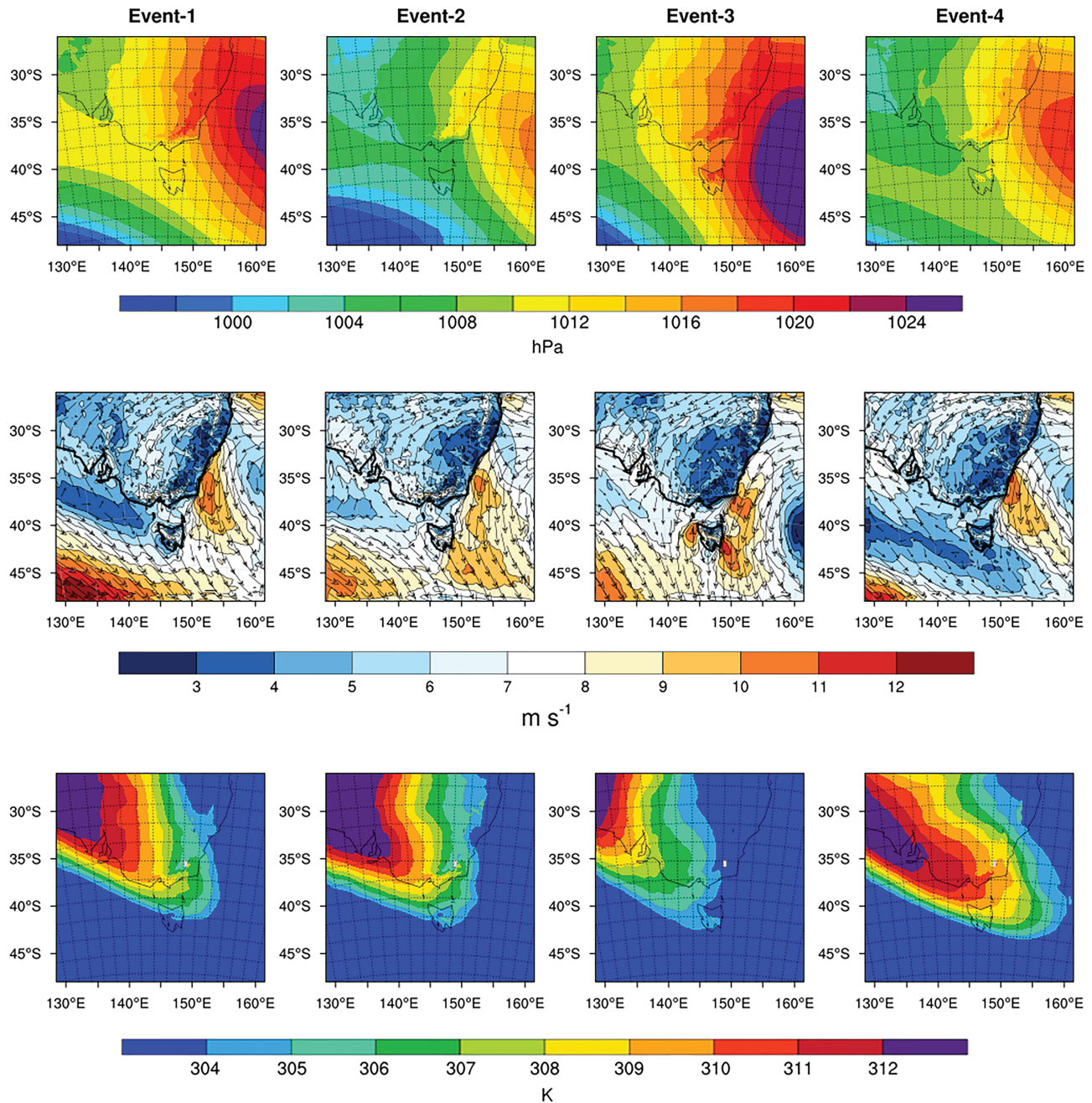## 2.5 | Human thermal comfort (HTC) calculation

This study also examines the impacts of urban expansion on the pedestrian level (approximated as above 2 m from ground level) human thermal comfort (HTC), characterized by the Universal Thermal Climate Index (UTCI) (Brode *et al.*, 2012). Although there are a number of indices used to calculate the HTC (for example, the discomfort index, the approximate wet-bulb globe temperature, and the

physiological equivalent temperature), the UTCI has been used as a thermal index of HTC in several studies (for example, Coutts *et al.*, 2016; Vatani *et al.*, 2016). The UTCI is a physiological response index in representing human bioclimatic conditions and their relevance to human thermal stress under different climatic conditions, which makes this index universal in nature, and it represents the temporal variability of thermal conditions better than other indices (Blazejczyk *et al.*, 2012). In this study, the radiation and human bioclimatic model Rayman Pro version 3.1 (Matzarakis *et al.*, 2007; Matzarakis *et al.*, 2010) is used for calculating the UTCI index. The UTCI takes into consideration not only the effect of air temperature, but also wind speed, relative humidity, and incoming solar radiation (Johansson, 2006). These variables were taken from the WRF outputs at pedestrian level at 2 m except incoming solar radiation at surface level as input data to the Rayman model. The latter also requires several human thermal parameters, and a default activity factor of 0.80 W and clothing factor of 0.90 for a male of 35 years of age were used. Different values of the UTCI correspond to different physiological stresses as illustrated in Table 2 (Brode *et al.*, 2012). It should be noted that there are some limitations and assumptions when computing indices such as the UTCI from model outputs. Wind speed at 2 m has to be interpolated from 10 m, as models typically diagnose winds at 10 m for evaluation purposes. Additionally, the calculation assumes a person is always sunlit, which is not realistic in urban environments. Finally, temperatures at 2 m from models such as WRF are diagnosed using Monin–Li and Bou-Zeid (2013).

TABLE 2 Scale of universal thermal comfort index (UTCI) for different grades of human thermal perception and associated physiological stress (Brode *et al.*, 2012)

UTCI (°C)	Physiological stress
+9 to +26	No thermal stress
+26 to +32	Moderate heat stress
+32 to +38	Strong heat stress
+38 to +46	Very strong heat stress
> +46	Extreme heat stress

FIGURE 2 Mean sea-level pressure (top panel), wind speed (colored contours) and direction (middle panel), and potential temperature at 850 hPa (bottom panel) for the four heatwave events averaged over 72 hr, from the outermost domain (Figure 1)
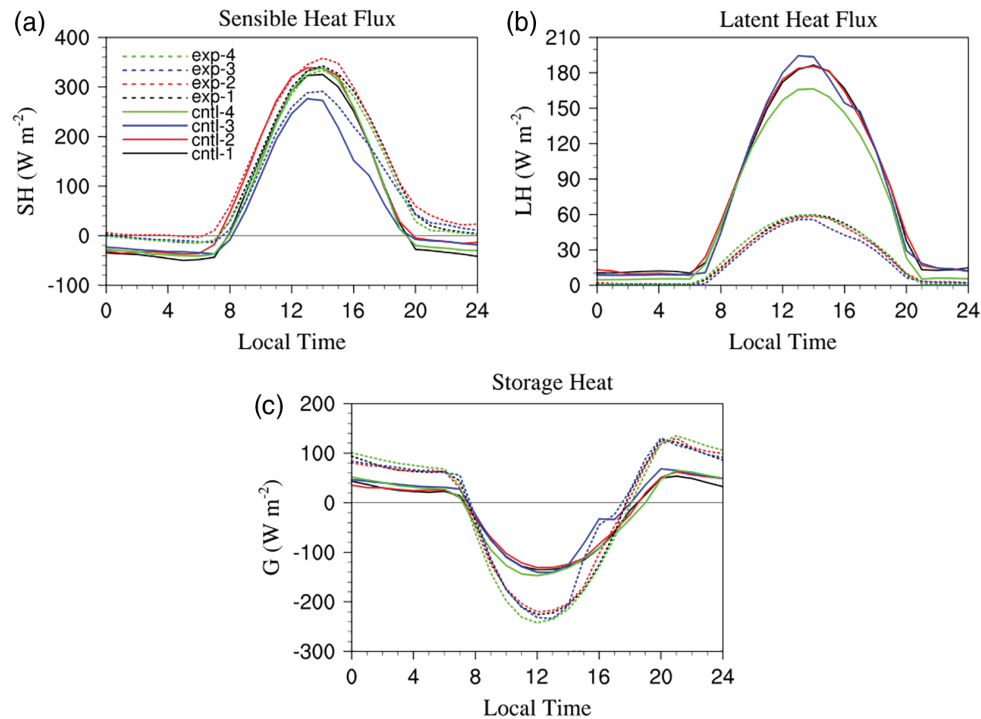
2.6 | Brief meteorology of the four heatwave events

Figure 2 shows the mean daily mean sea-level pressure (MSLP), wind speed with direction at 10 m, and potential temperature at 850 hPa from the outermost domain (Figure 1a). All four events were characterized by a strong anticyclone to the east and an approaching cold front from the southwest (top panel). The anticyclone resulted in the advection of hot and humid air from north and northeast (middle and bottom panels). This north/northeasterly wind flow resulted in very hot conditions throughout the

lower atmosphere (bottom panel), with potential temperatures reaching a maximum of 310–312 K during event 4 over large parts of southeast Australia.
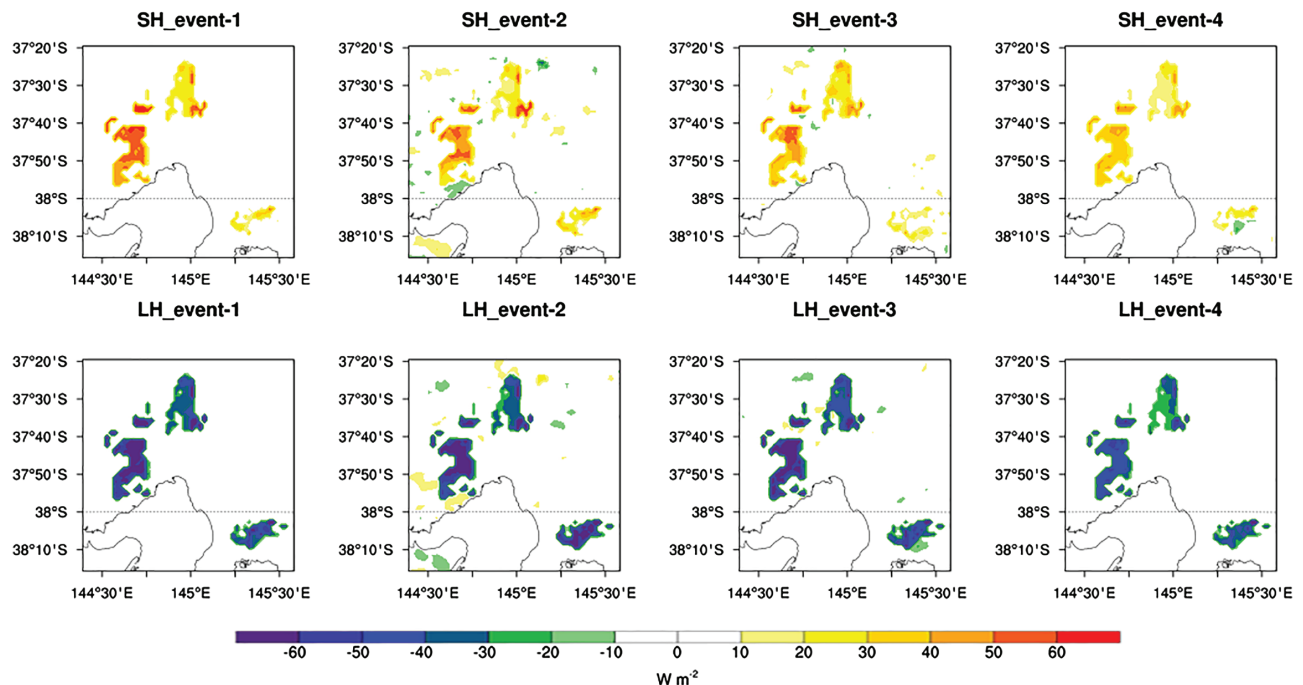
3 | RESULTS

3.1 | Impacts of high-density urban expansion on the surface energy balance

The diurnal cycle of the surface energy balance is shown in Figure 3 for the control (solid lines) and experiments (dotted lines) with urban expansion, averaged over urban grid
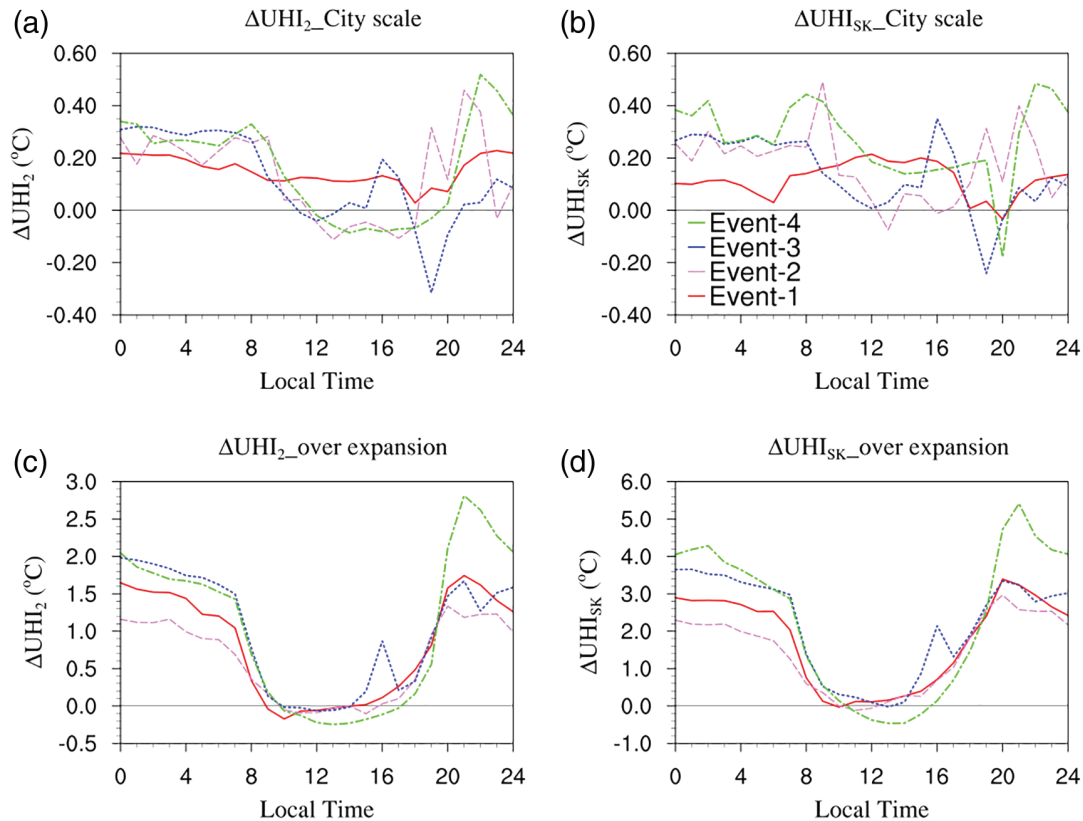
FIGURE 3 Diurnal cycle of the surface energy balance for control simulations (solid lines) and experiments (dotted lines) for the four heatwave events, averaged over expanded urban grid cells only (Figure 1c)

FIGURE 4 Changes (experiment minus control) in daily mean sensible (SH, top panels) and latent fluxes (LH, bottom panels) due to urban expansion for the four events, averaged over 72 hr

cells only. Urban expansion results in higher sensible heat flux during both the day and night for all events. The differences range from 70–80 W/m² during the evening between 1800 and 1900 local time, while early-morning peaks range from 22–35 W/m² for the four events. Urban expansion results in a large reduction of latent heat flux for all events, with

the maximum reduction occurring at 1300 local time, and varying between 100 and 140 W/m² among the four events, which is a much larger change in magnitude compared with the increase in sensible heat flux. The reduction in latent heat flux and higher thermal capacity of urban surfaces lead to enhanced storage heat for all events (Figure 3c). A positive

FIGURE 5 Changes in diurnal (a) UHI$_2$ (UHI at 2 m above the ground) and (b) UHI$_{sk}$ (surface UHI) averaged over all urban grid cells (original plus expanded), and (c) UHI$_2$ and (d) UHI$_{sk}$ averaged over the expanded urban areas only (Figure 1c)
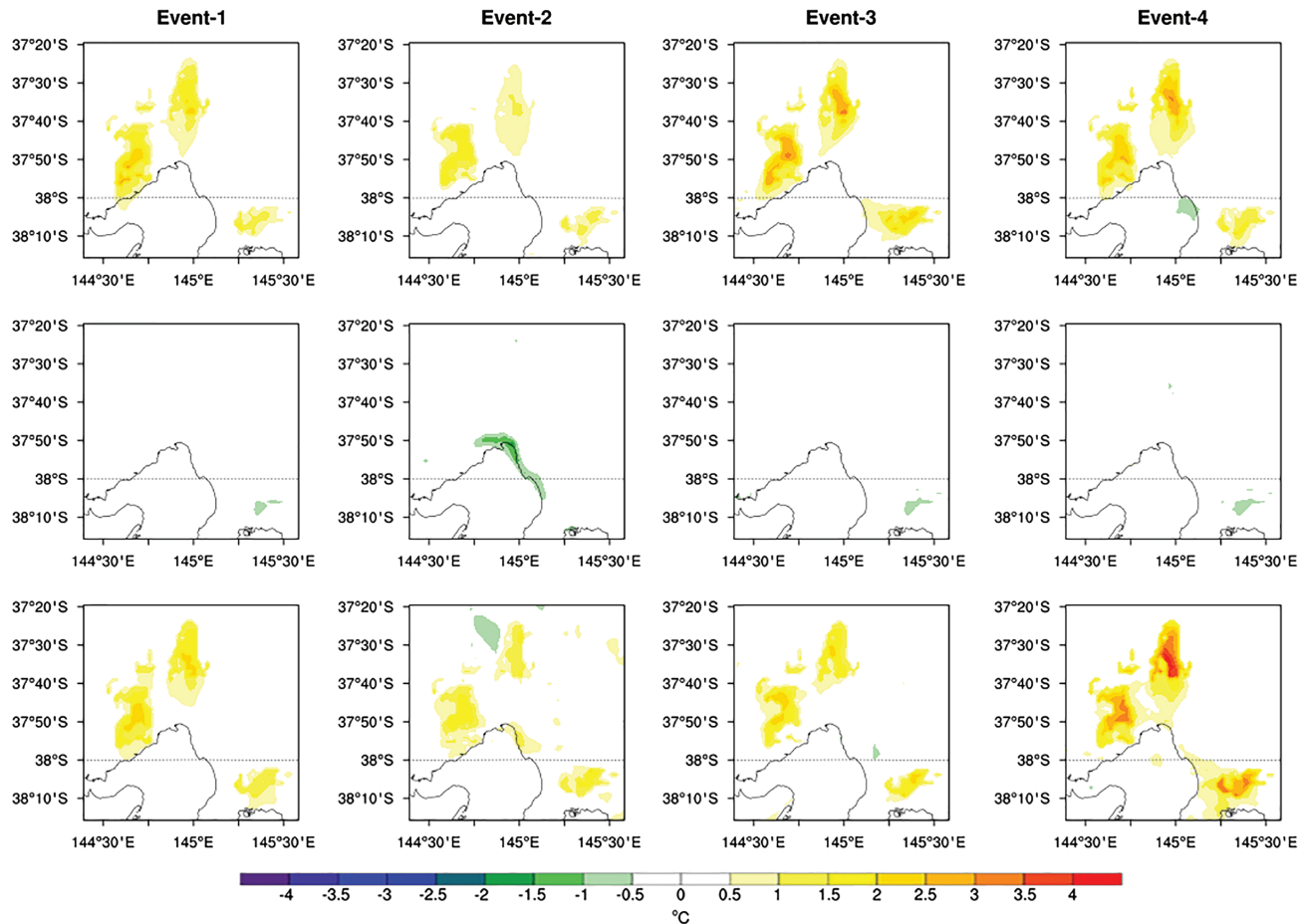
sign of storage heat indicates the flow of heat from the surface to the atmosphere and vice versa for negative storage heat. Urban expansion results in a maximum reduction in storage heat of 90 W/m^2 for the four events at 1200 local time, while the storage heat increases by nearly 50 and 70 W/m^2 during the morning and the night, respectively.

The spatial changes (experiment minus control) in daily mean sensible and latent heat fluxes are shown in Figure 4 (note that daily mean changes in storage heat are not shown in Figure 4, but are discussed in more detail in later in the article in Figure 10, as changes are of opposite sign during the day and night and hence are shown separately). The increase in sensible heat flux ranges from 50–70 W/m^2 in the western part of the city of Melbourne for the four events, while areas to the north and southeastern parts of the city show an increase of between 20 and 40 W/m^2. The latent heat flux reductions range from 50–70 W/m^2 in most areas over the expanded areas in the western and southeastern part of the city of Melbourne. The areas to the north show reductions in latent heat flux of 30–50 W/m^2. Urban expansion results in slightly smaller changes in sensible and latent heat fluxes during event 4 compared with all other events. This is likely due to this heatwave event being the driest and hottest of all four events. For events 2 and 3, the changes in sensible and latent heat fluxes extend to surrounding non-urban areas and this is explored further in Section 4).

3.2 | Impacts of high-density urban expansion on the near-surface and skin-surface UHI

Figure 5a,b show the influence of urban expansion on the near-surface urban heat island (UHI$_2$) and skin-surface urban heat island (UHI$_{sk}$) at the city scale (averaged over original and expanded urban grid cells across the domain), and Figure 5c,d show the same variables but averaged over the expanded urban areas only (Figure 1c). Urban expansion increases UHI$_2$ and UHI$_{sk}$ at the city scale and over expanded urban areas. The maximum UHI intensity for near-surface and skin surface is highest during the night both at the city scale and over expanded urban areas. At the city scale, UHI$_2$ increases by 0.20–0.35 °C during the morning and 0.10–0.50 °C during the night, while UHI$_{sk}$ increases by 0.10–0.40 °C and 0.10–0.50 °C during the morning and night, respectively. Furthermore, UHI$_2$ increases by 1.2–2 °C during the morning and 1–2.8 °C during the night over the expanded urban areas, but such large changes are not observed at the city scale. The effect of urban expansion is greater on UHI$_{sk}$ than on UHI$_2$, with UHI$_{sk}$ ranging from 2.2–4.1 °C during the morning and 2–5.4 °C during the night over expanded urban areas only. Interestingly, event 4 showed the highest change in UHI$_2$ and UHI$_{sk}$ during both morning and night, both at the city scale and over expanded areas, likely due to the drier and

FIGURE 6 Changes (experiment minus control) in mean T_2 (experiment minus control) due to urban expansion for the four events. The top row shows the results before sunrise (0200–0600 local time), the middle row shows the results when the effect of ΔUHI_2 is minimum (1000–1400 local time), and the bottom row shows the results when the effect of ΔUHI_2 is maximum (2000–2400 local time)
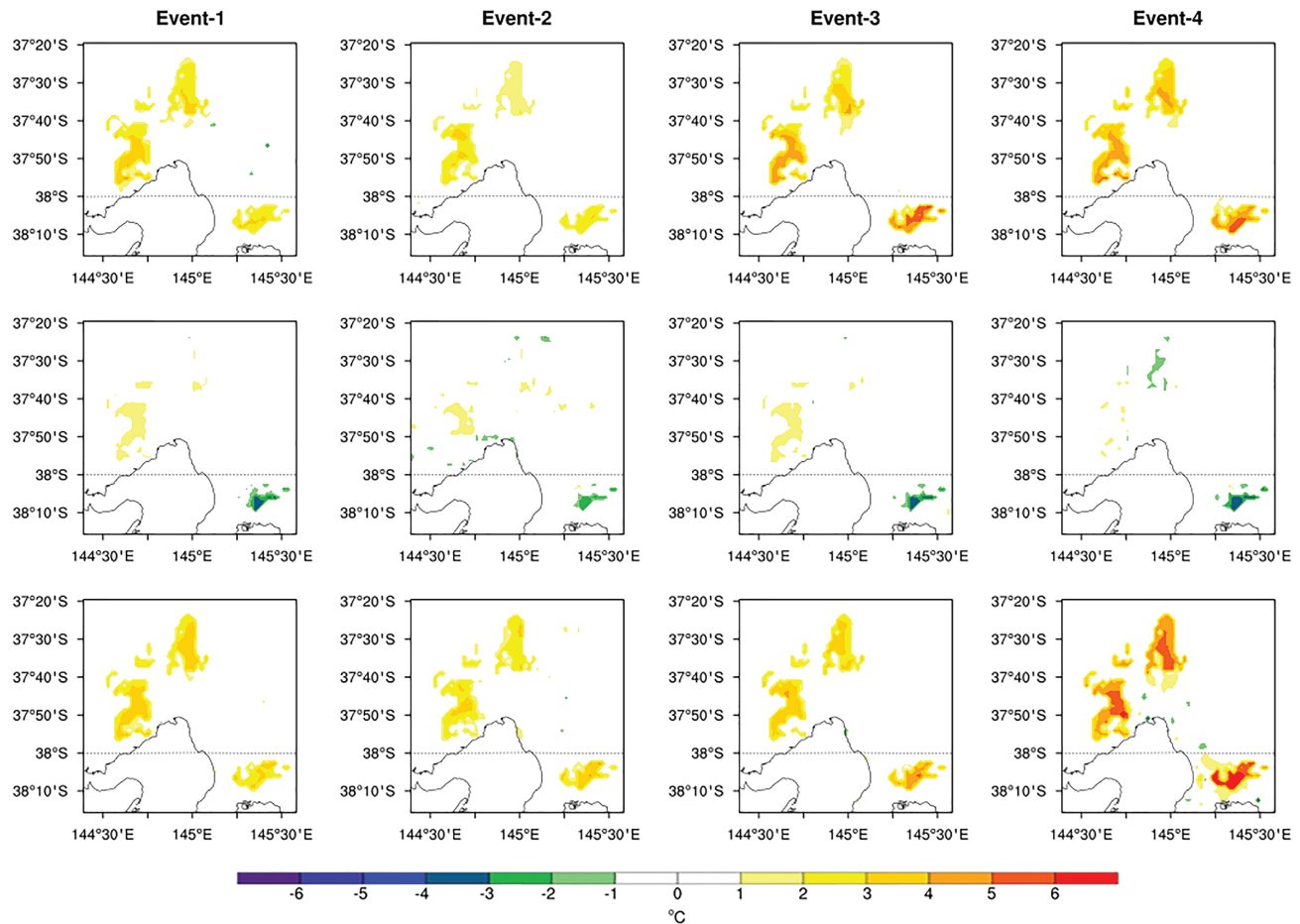
more severe heatwave characteristics among the four heatwave events. All events showed a lower change in UHI_2 and UHI_{sk} between 0900 and 1600 local time over expanded urban areas only.

The spatial changes (experiment minus control) in mean near-surface (T_2) and skin-surface (T_{sk}) temperatures are shown in Figures 6 and 7, respectively, averaged over three different time intervals 0200–0600 (before sunrise), 1000–1400 (when the change in UHI_2 and UHI_{sk} is minimum), and 2000–2400 local time (when the change in UHI_2 and UHI_{sk} is maximum) for the four events. T_2 increases by between 1.0 and 3.0 °C before sunrise and by 1.0 and 4.5 °C from evening to midnight, while events 3 and 4 show the warmest conditions as compared to events 1 and 2 (Figure 6). No substantial changes in T_2 are evident during the day (middle row) for all four events. The increases in T_{sk} (Figure 7) are higher than those in T_2, ranging between 1.0 and 7.0 °C for all four events before sunrise and between 2000 and 2400 local time when the maximum changes in UHI_2 and UHI_{sk} occur. Similarly to changes in T_2, changes in T_{sk} are not substantial during the day. It is also important to note that the high-density urban expansion extends the change in T_2 and

T_{sk} to the surrounding areas before sunrise and from evening to midnight. Event 4 shows the highest changes in T_2 and T_{sk}, due to high-density urban expansion, compared with the other three events before sunrise and after sunset. The changes in mean T_2 and T_{sk} during these three time periods were driven largely by changes in the minimum T_2 and T_{sk} over these periods, rather than the mean (Supporting information, Figures S1 and S2).

The spatial distributions of changes in mean storage heat flux, wind speed at 10 m, and relative humidity averaged over the different times (before sunset, during the day, and after sunset) are shown in Figures 8 and 9 (Figure S3), respectively. These were examined to help explore the physical processes and dynamics associated with the causes of higher intensity of UHI_2 and UHI_{sk} during the morning and night. Upward storage heat flux (positive storage heat) increases from 20 to 60 W/m^2 before sunrise and 40 to 80 W/m^2 during the evening for all events. On the other hand, downward/absorbed storage heat flux (negative storage heat) increases from 50 to 100 W/m^2 during the day for all events. The magnitude of increased storage heat is higher during the evening compared with the increased storage heat before sunrise. The changes in

FIGURE 7 Changes in mean T_{sk} (experiment minus control) due to urban expansion for the four events. The top row shows the results before sunrise (0200–0600 local time), the middle row shows the results when the effect of ΔUHI_{sk} is minimum (1000–1400 local time), and the bottom row shows the results when the effect of ΔUHI_{sk} is maximum (2000–2400 local time)
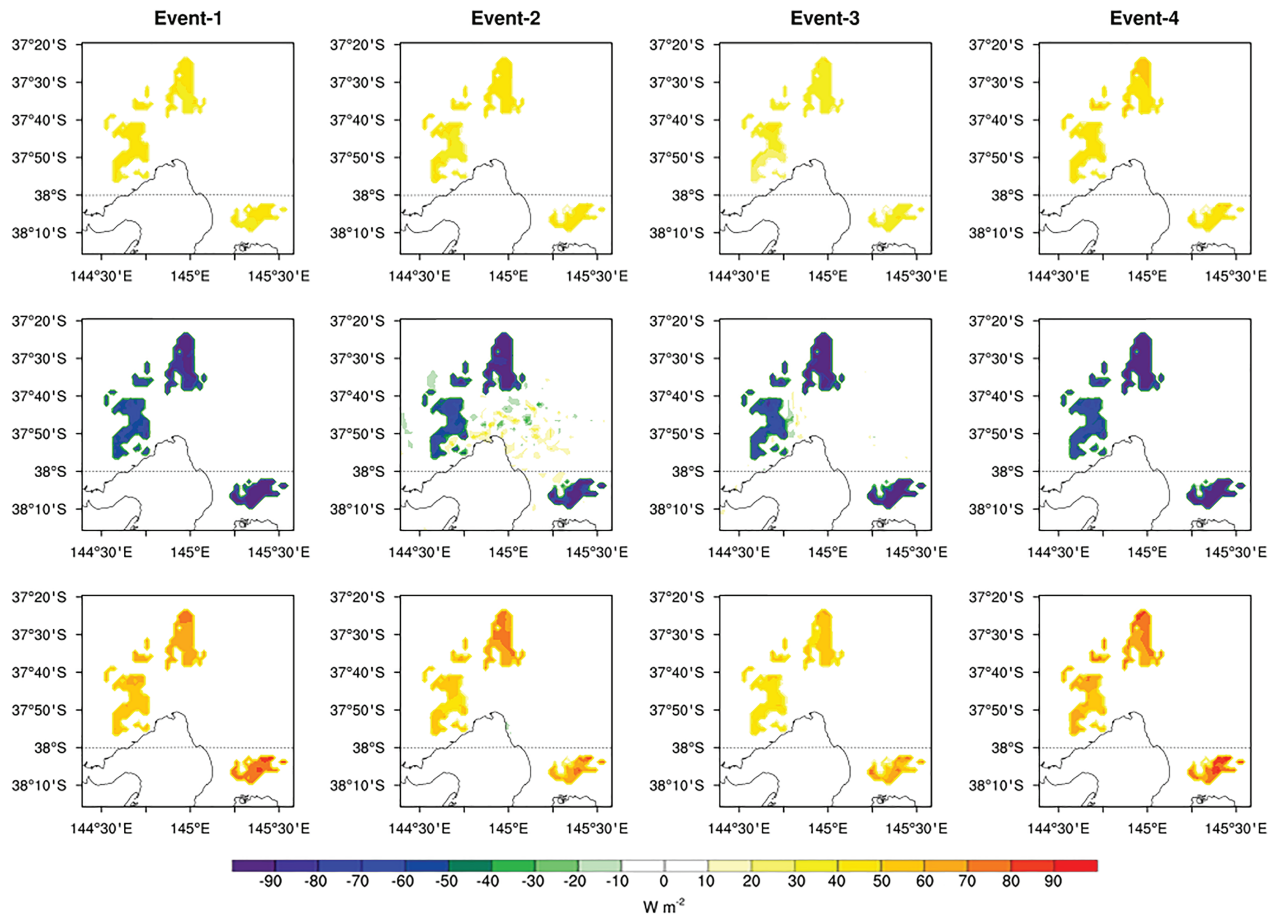
T_2 and T_{sk} are therefore driven largely by the changes in storage heat flux. During the day, urban expansion results in more heat storage, which is released at night. Since there were no changes in wind direction, but only in wind speed, Figure 9 shows the changes of wind speed (experiment minus control), and the wind barbs show the wind direction for the experiments only. The wind was predominantly northerly during both day and night for all events, with wind speed reductions from 1.0–4.0 m/s, especially during the day. The reductions of wind speed were slightly higher during the day compared with reductions of wind speed before sunrise and during the evening.

3.3 | Impacts of urban expansion within the boundary layer

The planetary boundary layer plays an important role in the transport and mixing of fluxes of heat and moisture. The changes in potential temperature within the boundary layer are shown in Figure 10. Urban expansion increases the potential temperatures by between 0.4 and 1.4 °C in the lower PBL (<300 m) between the evening and morning for all events,

and potential temperature decreases from 0.2 to 1.0 °C in the upper PBL (>300 m) both during day and night, especially for events 2 and 4. Event 2 showed the largest changes within the boundary layer compared with all other events, showing that the magnitude of the response to future urban expansion depends on the event, especially within the middle and upper boundary layer. Changes in PBL height were small (not shown), and only showed a slight increase during both the day and night, peaking in the evening.

Figure 11 (Figure S4) is similar to Figure 10 but shows the effect of urban expansion on wind speed and relative humidity within the boundary layer, respectively. Urbanization results in a reduction in wind speed by from 0.8 to 2.0 m/s in the lower boundary layer (<300 m) for all events, mostly during the night, because the wind was obstructed by the higher roughness (0.50) of urban structures compared with the roughness of replaced vegetated surfaces, particularly dry cropland and grassland (0.05–0.12). In the upper boundary layer (>300 m), wind speed increases from 0.8 to 2.5 m/s, especially for events 2 and 3. This increase in wind speed in the upper boundary likely occurs due to an increased pressure gradient because of the decrease in temperature in the upper layer.

FIGURE 8 Changes in storage heat (experiment minus control) due to urban expansion for the four events. The top row shows the results before sunrise (0200–0600 local time), the middle row shows the results when ΔUHI_2 and ΔUHI_{sk} are minimum (1000–1400 local time), and the bottom row shows the results when ΔUHI_2 and ΔUHI_{sk} are maximum (2000–2400 local time)
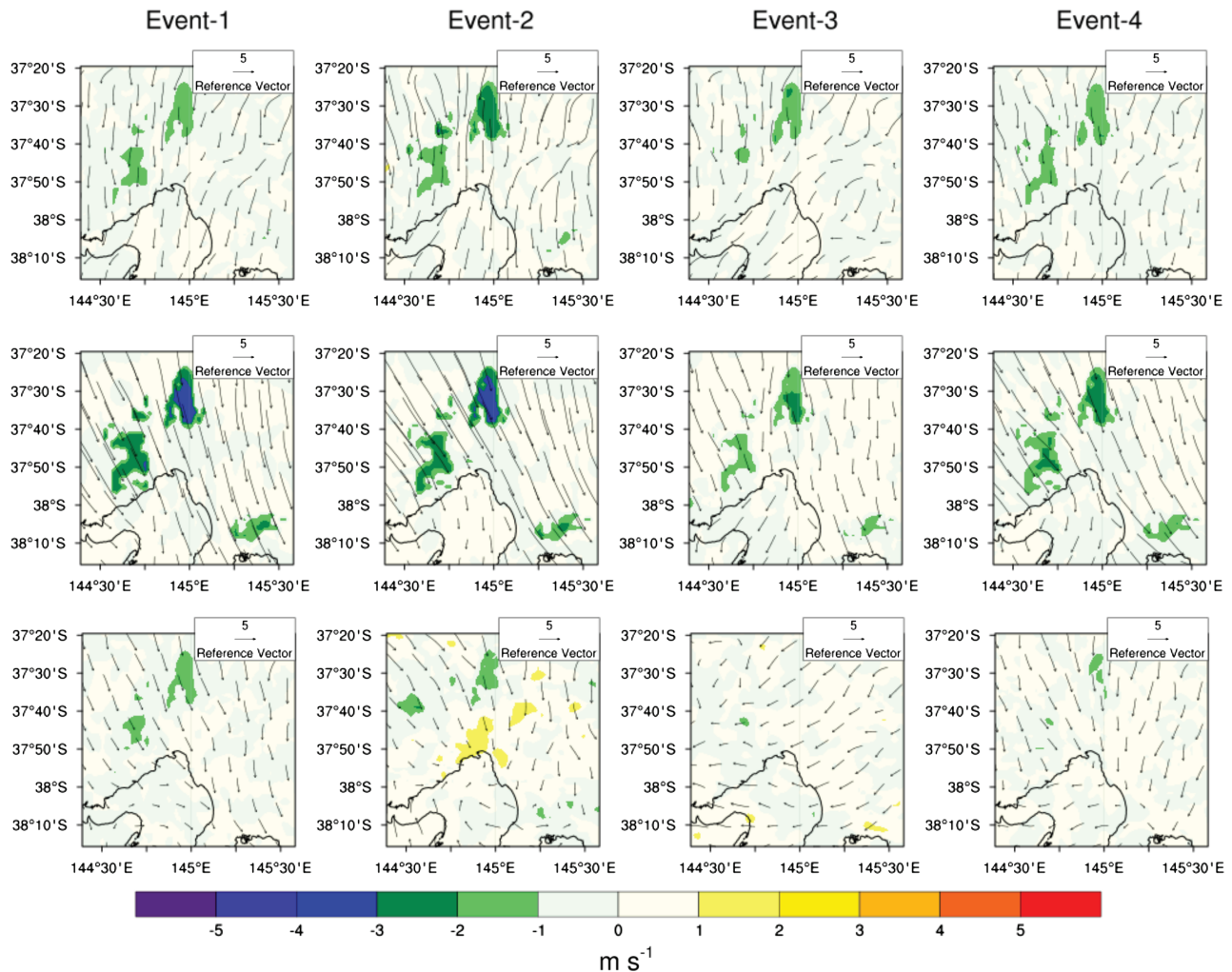
3.4 | Impacts on human thermal comfort

The hourly variations in UTCI at pedestrian level (approximated as 2 m above ground level) are assessed as a thermal index of HTC over three days for the four events. A higher UTCI index indicates a decrease in HTC and vice versa. Figure 12 (top) shows the hourly variation in the UTCI for the four control experiments, in which the strongest human thermal stress occurs between midday and afternoon, and the most severe human thermal stress occurred during event 4. We next examined the differences in UTCI between existing plus expanded urban areas and existing areas. The differences were very small ($+1$ to $-1\,°C$, not shown), which indicated that urban expansion did not have a strong influence on the UTCI over existing urban areas. We also examined the differences in UTCI between the expanded and existing urban area, as shown in Figure 12 (bottom). The expanded urban area has slightly lower UTCI (1–$2.5\,°C$) between 10.00 and 17.00 local time compared with existing urban areas, but higher UTCI between 1 and $5\,°C$ from evening to morning (1800 to 1000 local time), when the UTCI is generally at its lowest. The increase in UTCI during the night resulted in poorer HTC, which was driven by the storage heat due to higher urban

fractions (0.90) for high-density urban use in the expanded urban areas, compared with existing urban areas, which consist of both low- and high-density urban (Figure 1). For event 4, the most severe event, the increase in UTCI during this period results in an increase in human thermal stress from moderate to strong, but overall this increase in UTCI does not lead to a marked deterioration in HTC.

4 | DISCUSSION AND CONCLUSIONS

Previous studies have investigated the impacts of future urbanization in the city of Melbourne and other Australian cities (Coutts *et al.*, 2008; Argüeso *et al.*, 2014); however, no studies have investigated the impacts of future urbanization on the UHI during heatwave events, when health impacts are likely to be the most severe. Additionally, these studies were based on older policies, namely plan Melbourne 2030, and the release of plan Melbourne 2050 calls for an updated assessment of the impacts of future urbanization. Our results show that urban expansion substantially affects the surface energy balance by converting vegetated surfaces to impervious surfaces, which limits the availability of soil moisture and
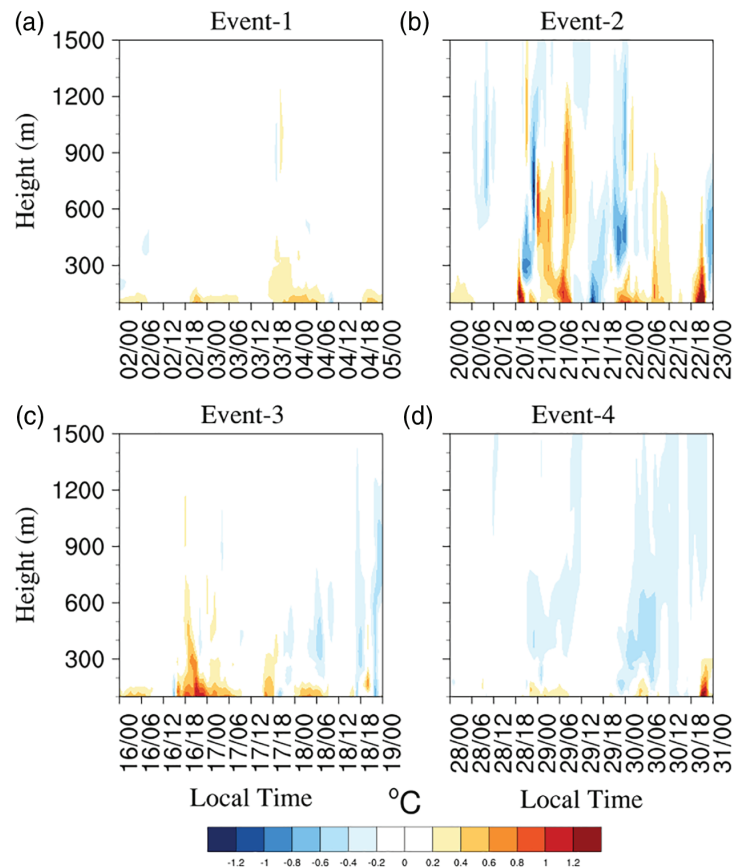
FIGURE 9 Wind direction from the experiment only, as shown by the wind vectors, and changes in wind speed (experiment minus control) due to urban expansion for four events, shown as filled color contours. The top row shows the results before sunrise (0200–0600 local time), the middle row shows the results when ΔUHI_2 and ΔUHI_{sk} are minimum (1000–1400 local time), and the bottom row shows the results when ΔUHI_2 and ΔUHI_{sk} are maximum (2000–2400 local time)

evapotranspiration and affects the partitioning of surface heat fluxes by increasing sensible heat flux and decreasing latent heat flux. Liu *et al.* (2018) and Argueso *et al.* (2014) report similar results in their studies, and show that urban expansion leads to a substantial increase in sensible heat flux and decrease in latent heat flux. Urban surfaces lead to an increase in sensible heat flux during the day compared with vegetated surfaces, because of a lack of evapotranspiration and trapping of solar radiation within the urban canopy. As the urban expansion replaces vegetated surfaces by impervious urban surfaces, the reduction in evapotranspiration and soil moisture reduces the latent heat flux, (Figure 3a,b and Figure 4), because the western suburbs of Melbourne city are climatologically drier and less densely forested compared with the eastern suburbs (Jacobs *et al.*, 2018). Therefore, the land cover and climatic conditions appear to play an important role in the reduction of latent heat flux and increase of sensible flux. However, these changes in sensible and latent heat fluxes do

not influence the UHI directly, though the storage heat flux plays a more important role.

There was a substantial increase in storage heat over the expanded urban areas, but no change in the surrounding areas. Absorption of solar radiation by urban surfaces increases the storage heat during the day compared with vegetated surfaces, due to higher conductivity and heat storage capacity of the construction materials (Li *et al.*, 2015; Morris *et al.*, 2011; Liu *et al.*, 2018). As a result, negative storage heat flux (from the atmosphere to surface) increases during the day, while positive storage heat (from the surface to atmosphere) increases between evening and morning. All four heatwave events showed the same overall response, that is, enhanced storage heat in urban surfaces during the day, because of extreme hot and dry weather conditions, which are released at night. Event 4, being the most severe, showed the largest response overall. Since the incoming solar radiation is more intense during heatwaves compared with usual summer days (Wang

FIGURE 10 Changes (experiment minus control) in hourly potential temperatures within the planetary boundary layer for (a) event 1, (d) event 2, (c) event 3, and (d) event 4, averaged over all urban grid cells in the expanded urban areas only

et al., 2017; Liu *et al.*, 2018), higher urban fractions of urban surfaces absorb and store more solar heat, and consequently intensify the nocturnal UHI_2 and UHI_{sk} (Figure 5). The stored heat is slowly released during the night until morning (Coutts *et al.*, 2007; Wang *et al.*, 2017; Liu *et al.*, 2018), and therefore urban expansion intensifies the nocturnal UHI_2 and UHI_{sk} (Figure 5) and also leads to a substantial increase in mean near-surface (Figure 6) and skin surface (Figure 7) temperatures and minimum near-surface (Figure S1) and skin-surface (Figure S2) temperatures during the night, particularly from evening to morning.
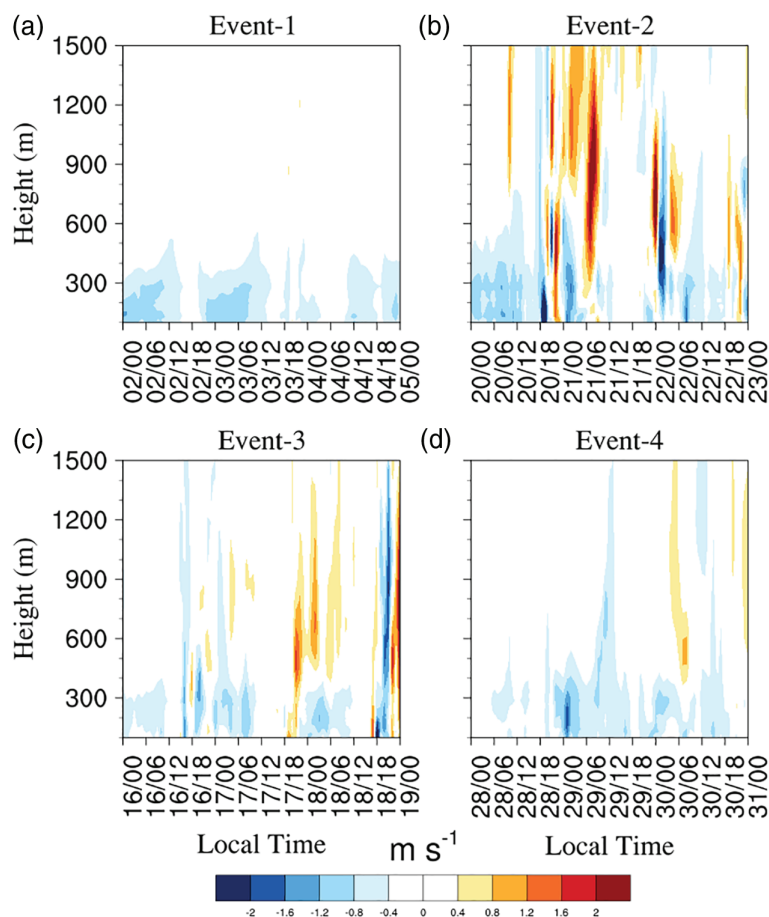
It is noteworthy that there were no substantial UHI effects during the day. The likely reason is that both urban and vegetated surfaces were heated by intense solar radiation with drier weather conditions due to heatwaves during the day, which dominated the fluxes over urban and vegetated areas and reduced the thermal difference between these two areas (Liu *et al.*, 2018). Another important finding of this study is that increases in the mean temperature before sunrise, between 1000–1400 and 2000–2400, were driven by changes in the minimum between these time intervals. Dry and hot inland winds from north (inland) to south (ocean) extend the UHI_2 beyond the expanded areas, although there was an overall reduction in wind speed near the surface. The changes in wind speed are unlikely to have a large impact on T_2 and

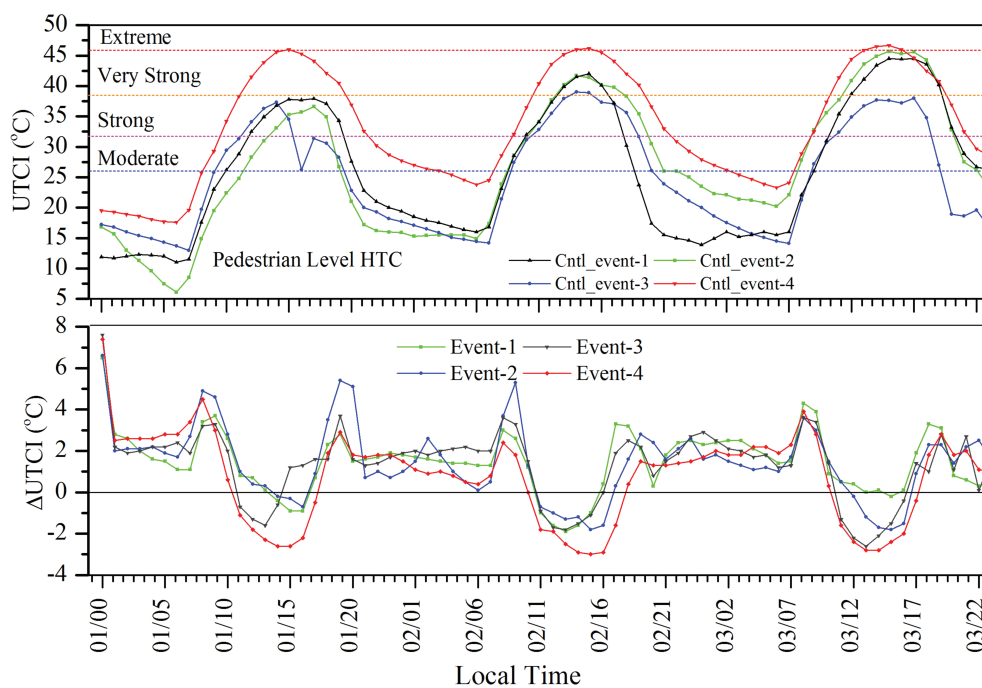T_{sk}, as the reductions in wind speed were fairly small for all events.

Urban expansion had a substantial influence on the potential temperature within the lower boundary layer, particularly during the evening and night, due to higher heat storage by urban surfaces. The increase in potential temperatures decreased with increasing PBL height, which is consistent with Yang *et al.* (2016), who showed lower potential temperature with increasing PBL height due to urbanization. Urban expansion did not increase human thermal stress in existing urban areas, and differences in UTCI between the existing and expanded urban areas were not large enough, except for the most severe event from evening to morning, when the UTCI is low. It is noteworthy that the hourly variations in UTCI follow the variations of diurnal cycles of UHI_2, which are driven by the increase in storage heat. Therefore, storage heat due to higher urban fractions in expanded urban areas plays a crucial role in deteriorating HTC during the night.

Finally, this study has some limitations, which need to be discussed. The impacts of future climate change on future urban expansion are not considered, as the simulations including urban expansion are driven with the ERA-Interim reanalysis data, since this study is based on real case studies. Future warming will likely exacerbate UHI effects further

FIGURE 11 Changes (experiment minus control) in hourly wind speed within the planetary boundary layer for (a) event 1, (d) event 2, (c) event 3, and (d) event 4, averaged over all urban grid cells in the expanded urban areas only

FIGURE 12 Hourly variation in pedestrian level UTCI from the control simulations for 3 days (top), and changes (expansion minus existing urban areas) in hourly UTCI (bottom)

if there is no mitigation, and therefore the effects of future urban expansion are likely to be underestimated in this study. For example, Krayenhoff *et al.* (2018) showed that the combination of urban expansion and future climate change is likely to increase summertime urban warming by 1–6 K in the afternoon and 3–8 K at night by the end of the century. These ranges of warming are larger than our results for increases in near-surface temperature due to urban expansion alone. We also acknowledge that the use of constant urban fractions, road fractions, building heights, and so on, for each of the three urban categories is unlikely to be truly representative of the city of Melbourne. This study evaluated the impacts of high-density urban expansion using a constant urban fraction for all future expansion, to investigate the maximum possible response, rather than the expected response. Offline simulations with the Noah land-surface model for the city of Houston, USA, have shown that specifying the urban fraction explicitly for each grid cell, as opposed to using constant values for each urban land-use category, yielded more accurate simulations of the surface radiative temperature (Monaghan *et al.*, 2014). Therefore, future studies should investigate the use of spatially varying urban properties versus constant values. Finally, this study is limited by the use of a single urban canopy model, WRF-SLUCM, and more robust assessments of the impacts of future urbanization should make use of multiple urban canopy models.

ORCID

Hosen M. Imran https://orcid.org/0000-0001-7083-8747

REFERENCES

Adachi, S.A., Kimura, F., Kusaka, H., Duda, M.G., Yamagata, Y., Seya, H. and Aoyagi, T. (2014) Moderation of summertime heat island phenomena via modification of the urban form in the Tokyo metropolitan area. *Journal of Applied Meteorology and Climatology*, 53(8), 1886–1900. https://doi.org/10.1175/jamc-d-13-0194.1.

Argüeso, D., Evans, J.P., Fita, L. and Bormann, K.J. (2014) Temperature response to future urbanization and climate change. *Climate Dynamics*, 42(7), 2183–2199. https://doi.org/10.1007/s00382-013-1789-6.

Arnfield, A.J. (2003) Two decades of urban climate research: a review of turbulence, exchanges of energy and water, and the urban heat island. *International Journal of Climatology*, 23(1), 1–26. https://doi.org/10.1002/joc.859.

Australian Bureau of Statistics (2008) ABS 3222.0 Population projections, Australia 2006 to 2101. Available at: http://www.abs.gov.au/Ausstats/abs@.nsf/Latestproducts/3222.0 [Accessed 7 August 2018].

Blazejczyk, K., Epstein, Y., Jendritzky, G., Staiger, H. and Tinz, B. (2012) Comparison of UTCI to selected thermal indices. *International Journal of Biometeorology*, 56(3), 515–535. https://doi.org/10.1007/s00484-011-0453-2.

Block, A.H., Livesley, S.J. and Williams, S.J. (2012) Responding to the urban heat island: a review of the potential of green infrastructure. Available at: http://www.vcccar.org.au/sites/default/files/publications/VCCCAR%20Urban%20Heat%20Island%20-WEB.pdf [Accessed 5 July 2018]

Brode, P., Fiala, D., Błazejczyk, K., Holmer, I., Jendritzky, G., Kampmann, B., Tinz, B. and Havenith, G. (2012) Deriving the operational procedure for the universal thermal climate index (UTCI). *International Journal of Biometeorology*, 56(3), 481e494. https://doi.org/10.1007/s00484-011-0454-I.

Chen, F. and Dudhia, J. (2001) Coupling an advanced land surface–hydrology model with the Penn state–NCAR MM5 modeling system. Part I: model implementation and sensitivity. *Monthly Weather Review*, 129(4), 569–585. https://doi.org/10.1175/1520-0493(2001)129<0569:caalsh>2.0.co;2.

Chen, F., Yang, X. and Zhu, W. (2014) WRF simulations of urban heat island under hot-weather synoptic conditions: the case study of Hangzhou City, China. *Atmospheric Research*, 138, 364–377. https://doi.org/10.1016/j.atmosres.2013.12.005.

Chen, L. and Frauenfeld, O.W. (2016) Impacts of urbanization on future climate in China. *Climate Dynamics*, 47(1), 345–357. https://doi.org/10.1007/s00382-015-2840-6.

Coates, L., Haynes, K., O'Brien, J., McAneney, J. and de Oliveira, F.D. (2014) Exploring 167 years of vulnerability: an examination of extreme heat events in Australia 1844–2010. *Environmental Science & Policy*, 42, 33–44. https://doi.org/10.1016/j.envsci.2014.05.003.

Coutts, A.M., Beringer, J. and Tapper, N.J. (2007) Impact of increasing urban density on local climate: spatial and temporal variations in the surface energy balance in Melbourne, Australia. *Journal of Applied Meteorology and Climatology*, 46(4), 477–493.

Coutts, A.M., Beringer, J. and Tapper, N.J. (2008) Investigating the climatic impact of urban planning strategies through the use of regional climate modelling: a case study for Melbourne, Australia. *International Journal of Climatology: A Journal of the Royal Meteorological Society*, 28(14), 1943–1957.

Coutts, A.M., White, E.C., Tapper, N.J., Beringer, J. and Livesley, S.J. (2016) Temperature and human thermal comfort effects of street trees across three contrasting street canyon environments. *Theoretical and Applied Climatology*, 124(1), 55–68. https://doi.org/10.1007/s00704-015-1409-y.

Dee, D.P., Uppala, S.M., Simmons, A.J., Berrisford, P., Poli, P., Kobayashi, S., Andrae, U., Balmaseda, M.A., Balsamo, G., Bauer, P., Bechtold, P., Beljaars, A.C.M., van de Berg, L., Bidlot, J., Bormann, N., Delsol, C., Dragani, R., Fuentes, M., Geer, A.J., Haimberger,

L., Healy, S.B., Hersbach, H., Hólm, E.V., Isaksen, L., Kållberg, P., Köhler, M., Matricardi, M., McNally, A.P., Monge-Sanz, B.M., Morcrette, J.J., Park, B.K., Peubey, C., de Rosnay, P., Tavolato, C., Thépaut, J.N. and Vitart, F. (2011) The ERA-Interim reanalysis: configuration and performance of the data assimilation system. *Quarterly Journal of the Royal Meteorological Society*, 137(656), 553–597. https://doi.org/10.1002/qj.828.

Department of Infrastructure and Regional Development (2013) Australian State of the Cities 2013. Chapter 4 Sustainability Australian Government Available at: http://www.infrastructure.gov.au/infrastructure/pab/soac/ [Accessed 10th July 2018].

Engel, C.B., Lane, T.P., Reeder, M.J. and Rezny, M. (2013) The meteorology of Black Saturday. *Quarterly Journal of the Royal Meteorological Society*, 139(672), 585–599. https://doi.org/10.1002/qj.1986.

Frolking, S., Milliman, T., Seto, K.C. and Friedl, M.A. (2013) A global fingerprint of macro-scale changes in urban structure from 1999 to 2009. *Environmental Research Letters*, 8(2), 024004.

Grell, G.A. and Dévényi, D. (2002) A generalized approach to parameterizing convection combining ensemble and data assimilation techniques. *Geophysical Research Letters*, 29, 1693. https://doi.org/10.1029/2002GL015311.

Harman, I.N. and Belcher, S.E. (2006) The surface energy balance and boundary layer over urban street canyons. *Quarterly Journal of the Royal Meteorological Society*, 132, 2749–2768. https://doi.org/10.1256/qj.05.185.

Holt, T. and Pullen, J. (2007) Urban canopy modeling of the New York city metropolitan area: a comparison and validation of single- and multilayer parameterizations. *Monthly Weather Review*, 135(5), 1906–1930. https://doi.org/10.1175/mwr3372.1.

Hurley, P. (2000) Verification of TAPM meteorological predictions in the Melbourne region for a winter and summer month. *Australian Meteorological Magazine*, 49(2), 97–107.

Iacono, M.J., Delamere, J.S., Mlawer, E.J., Shephard, M.W., Clough, S.A. and Collins, W.D. (2008) Radiative forcing by long-lived greenhouse gases: Calculations with the AER radiative transfer models. *Journal of Geophysical Research: Atmospheres*, 113(1–8), D13103. https://doi.org/10.1029/2008JD009944.

Imran, H.M., Kala, J., Ng, A.W.M. and Muthukumaran, S. (2018a) Effectiveness of green and cool roofs in mitigating urban heat island effects during a heatwave event in the city of Melbourne in southeast Australia. *Journal of Cleaner Production*, 197, 393–405. https://doi.org/10.1016/j.jclepro.2018.06.179.

Imran, H.M., Kala, J., Ng, A.W.M. and Muthukumaran, S. (2018b) An evaluation of the performance of a WRF multi-physics ensemble for heatwave events over the city of Melbourne in southeast Australia. *Climate Dynamics*, 50(7), 2553–2586. https://doi.org/10.1007/s00382-017-3758-y.

Jackson, T.L., Feddema, J.J., Oleson, K.W., Bonan, G.B. and Bauer, J.T. (2010) Parameterization of urban characteristics for global climate modeling. *Annals of the Association of American Geographers*, 100(4), 848–865.

Jacobs, S.J., Gallant, A.J., Tapper, N.J. and Li, D. (2018) Use of cool roofs and vegetation to mitigate urban heat and improve human thermal stress in Melbourne, Australia. *Journal of Applied Meteorology and Climatology*, 57, 1747–1764. https://doi.org/10.1175/JAMC-D-17-0243.1.

Jacobs, S.J., Gallant, A.J.E. and Tapper, N.J. (2017) The sensitivity of urban meteorology to soil moisture boundary conditions: a case study in Melbourne, Australia. *Journal of Applied Meteorology and*

Climatology, 56(8), 2155–2172. https://doi.org/10.1175/jamc-d-17-0007.1.

Janjic, Z. (1994) The step-mountain eta coordinate model: further developments of the convection, viscous sublayer, and turbulence closure schemes. *Monthly Weather Review*, 122, 5.

Johansson, E. (2006) Influence of urban geometry on outdoor thermal comfort in a hot dry climate: a study in Fez, Morocco. *Building and environment*, 41(10), 1326–1338.

Krayenhoff, E.S., Moustaoui, M., Broadbent, A.M., Gupta, V. and Georgescu, M. (2018) Diurnal interaction between urban expansion, climate change and adaptation in US cities. *Nat. Clim. Chang.*, 8, 1097–1103.

Kusaka, H., Kondo, H., Kikegawa, Y. and Kimura, F. (2001) A simple single-layer urban canopy model for atmospheric models: comparison with multi-layer and slab models. *Boundary-Layer Meteorology*, 101(3), 329–358.

Li, D. and Bou-Zeid, E. (2013) Synergistic interactions between urban heat islands and heat waves: the impact in cities is larger than the sum of its parts. *Journal of Applied Meteorology and Climatology*, 52(9), 2051–2064.

Li, D., Sun, T., Liu, M., Yang, L., Wang, L. and Gao, Z. (2015) Contrasting responses of urban and rural surface energy budgets to heat waves explain synergies between urban heat islands and heat waves. *Environmental Research Letters*, 10(5), 054009.

Liao, J., Wang, T., Wang, X., Xie, M., Jiang, Z., Huang, X. and Zhu, J. (2014) Impacts of different urban canopy schemes in WRF/Chem on regional climate and air quality in Yangtze River Delta, China. *Atmospheric Research*, 145–146, 226–243. https://doi.org/10.1016/j.atmosres.2014.04.005.

Liu, X., Tian, G., Feng, J., Ma, B., Wang, J. and Kong, L. (2018) Modeling the warming impact of urban land expansion on hot weather using the weather research and forecasting model: a case study of Beijing, China. *Advances in Atmospheric Sciences*, 35(6), 723–736. https://doi.org/10.1007/s00376-017-7137-8.

Matzarakis, A., Rutz, F. and Mayer, H. (2007) Modelling radiation fluxes in simple and complex environments – application of the RayMan model. *International Journal of Biometeorology*, 51(4), 323–334. https://doi.org/10.1007/s00484-006-0061-8.

Matzarakis, A., Rutz, F. and Mayer, H. (2010) Modelling radiation fluxes in simple and complex environments: basics of the RayMan model. *International Journal of Biometeorology*, 54(2), 131–139. https://doi.org/10.1007/s00484-009-0261-0.

Meng, W.G., Zhang, Y.X., Li, J.N., Lin, W.S., Dai, G.F. and Li, H.R. (2011) Application of WRF/UCMin the simulation of a heat wave event and urban heat island around Guangzhou. *Journal of Tropical Meteorology*, 17(3), 257–267. https://doi.org/10.3969/j.issn.1006-8775.2011.03.007.

Monaghan, A.J., Hu, L., Brunsell, N.A., Barlage, M. and Wilhelmi, O.V. (2014) Evaluating the impact of urban morphology configurations on the accuracy of urban canopy model temperature simulations with MODIS. *Journal of Geophysical Research: Atmospheres*, 119, 6376–6392. https://doi.org/10.1002/2013JD021227.

Morris, C.J.G. and Simmonds, I. (2000) Associations between varying magnitudes of the urban heat island and the synoptic climatology in Melbourne, Australia. *International Journal of Climatology*, 20(15), 1931–1954. https://doi.org/10.1002/1097-0088(200012)20:15<1931::AID-JOC578>3.0.CO;2-D.

Morris, K.I., Chan, A., Morris, K.J.K., Ooi, M.C.G., Oozeer, M.Y., Abakr, Y.A., Nadzir, M.S.M., Mohammed, I.Y. and Al-Qrimli, H.F. (2011) Impact of urbanization level on the interactions of urban area,

the urban climate, and human thermal comfort. *Applied Geography*, 79, 50–72. https://doi.org/10.1016/j.apgeog.2016.12.007.

Nairn, J. and Fawcett, R. (2011) *Defining Heatwaves: Heatwave Defined as a Heat-Impact Event Servicing*. All Community and Business Sectors in Australia. CAWCR technical report, ISSN 1835-9884. Available on http://www.bushfirecrc.com/sites/default/files/managed/resource/nairn_john.pdf [Accessed 7th July 2018].

Nicholls, N. and Larsen, S. (2011) Impact of drought on temperature extremes in Melbourne, Australia. *Australian Meteorological and Oceanographic Journal*, 61(2), 113–116.

Oke, T.R. (1981) Canyon geometry and the nocturnal urban heat island: comparison of scale model and field observations. *Journal of Climatology*, 1, 237–254. https://doi.org/10.1002/joc.3370010304.

Oke, T.R., Johnson, G.T., Steyn, D.G. and Watson, I.D. (1991) Simulation of surface urban heat islands under 'ideal' conditions at night. Part 2: Diagnosis of causation. *Boundary-Layer Meteorology*, 56, 339–358.

Pauleit, S., Ennos, R. and Golding, Y. (2005) Modeling the environmental impacts of urban land use and land cover change – a study in Merseyside, UK. *Landscape and Urban Planning*, 71(2), 295–310. https://doi.org/10.1016/j.landurbplan.2004.03.009.

Perkins-Kirkpatrick, S., White, C., Alexander, L., Argüeso, D., Boschat, G., Cowan, T. and Phatak, A. (2016) Natural hazards in Australia: heatwaves. *Climatic Change*, 139(1), 101–114.

Seto, K.C. and Shepherd, J.M. (2009) Global urban land-use trends and climate impacts. *Current Opinion in Environmental Sustainability*, 1(1), 89–95. https://doi.org/10.1016/j.cosust.2009.07.012.

Sharma, A., Conry, P., Fernando, H.J.S., Alan, F.H., Hellmann, J.J. and Chen, F. (2016) Green and cool roofs to mitigate urban heat island effects in the Chicago metropolitan area: evaluation with a regional climate model. *Environmental Research Letters*, 11(6), 064004.

Skamarock, W.C., Klemp, J.B., Dudhia, J., Gill, D.O., Barker, D.M., Wang, W. and Powers, J.G. (2005) *A Description of the Advanced Research WRF version 2*. Boulder, CO: National Center For Atmospheric Research Boulder Co Mesoscale and Microscale Meteorology Div.

Stone, B., Hess, J.J. and Frumkin, H. (2010) Urban form and extreme heat events: are sprawling cities more vulnerable to climate change than compact cities? *Environmental Health Perspectives*, 118(10), 1425–1428. https://doi.org/10.1289/ehp.0901879.

Thompson, G., Field, P.R., Rasmussen, R.M. and Hall, W.D. (2008) Explicit forecasts of winter precipitation using an improved bulk microphysics scheme. part ii: implementation of a new snow parameterization. *Monthly Weather Review*, 136(12), 5095–5115. https://doi.org/10.1175/2008mwr2387.1.

Torok, S.J., Morris, C.J.G., Skinner, C. and Plummer, N. (2001) Urban heat island features of southeast Australian towns. *Australian Meteorological Magazine*, 50, 1–13.

Vatani, J., Golbabaei, F., Dehghan, S.F. and Yousefi, A. (2016) Applicability of Universal Thermal Climate Index (UTCI) in occupational heat stress assessment: a case study in brick industries. *Industrial Health*, 54(1), 14–19. https://doi.org/10.2486/indhealth.2015-0069.

Wang, J., Feng, J., Yan, Z., Hu, Y. and Jia, G. (2012) Nested high-resolution modeling of the impact of urbanization on regional climate in three vast urban agglomerations in China. *Journal of Geophysical Research: Atmospheres*, 117(D21103), 1–18. https://doi.org/10.1029/2012JD018226.

Wang, J., Yan, Z., Quan, X.-W. and Feng, J. (2017) Urban warming in the 2013 summer heat wave in eastern China. *Climate Dynamics*, 48(9), 3015–3033. https://doi.org/10.1007/s00382-016-3248-7.

Wang, X., Sun, X., Tang, J. and Yang, X. (2015) Urbanization-induced regional warming in Yangtze River Delta: potential role of anthropogenic heat release. *International Journal of Climatology*, 35(15), 4417–4430. https://doi.org/10.1002/joc.4296.

Yang, L., Niyog, D., Tewari, M., Aliaga, D., Chen, F., Tian, F. and Ni, G. (2016) Contrasting impacts of urban forms on the future thermal environment: example of Beijing metropolitan area. *Environmental Research Letters*, 11, 034018. https://doi.org/10.1088/1748-9326/11/3/034018.

Zhao, C., Jiang, Q., Sun, Z., Zhong, H. and Lu, S. (2013) Projected urbanization impacts on surface climate and energy budgets in the pearl river delta of China. *Advances in Meteorology*, 2013, 10. https://doi.org/10.1155/2013/542086.

SUPPORTING INFORMATION

Additional supporting information may be found online in the Supporting Information section at the end of this article.